Jinst

Published by IOP Publishing for Sissa Medialab

Received: *October 11, 2016*
Accepted: *November 17, 2016*
Published: *December 7, 2016*

Pixel 2016 International Workshop
September 5 – September 9, 2016
Sestri Levante, Genova, Italy

The 4D pixel challenge

N. Cartiglia[a,1] **R. Arcidiacono,**[a,c] **A. Bellora,**[b] **F. Cenna,**[a,b] **R. Cirio,**[a,b] **S. Durando,**[b] **M. Ferrero,**[e] **P. Freeman,**[a,b] **Z. Galloway,**[e] **B. Gruey,**[e] **M. Mashayekhi,**[f] **M. Mandurrino,**[a,d] **V. Monaco,**[a,b] **R. Mulargia,**[a,b] **M. Obertino,**[a,b] **F. Ravera,**[a,b] **R. Sacchi,**[a,b] **H.F-W. Sadrozinski,**[e] **A. Seiden,**[e] **V. Sola,**[a] **N. Spencer,**[e] **A. Staiano,**[a] **M. Wilder,**[e] **N. Woods**[e] **and A. Zatserklyaniy**[e]

[a] *INFN Torino*
[b] *Università di Torino, Torino, Italy*
[c] *Università del Piemonte Orientale, Novara, Italy*
[d] *Politecnico di Torino, Torino, Italy*
[e] *Santa Cruz Institute for Particle Physics UC Santa Cruz, CA, 95064, U.S.A.*
[f] *Università di Sabzevar, Iran*

E-mail: cartiglia@to.infn.it

Abstract: Is it possible to design a detector able to concurrently measure time and position with high precision? This question is at the root of the research and development of silicon sensors presented in this contribution. Silicon sensors are the most common type of particle detectors used for charged particle tracking, however their rather poor time resolution limits their use as precise timing detectors. A few years ago we have picked up the gantlet of enhancing the remarkable position resolution of silicon sensors with precise timing capability. I will be presenting our results in the following pages.

Keywords: Instrumentation and methods for time-of-flight (TOF) spectroscopy; Particle tracking detectors (Solid-state detectors); Si microstrip and pad detectors; Timing detectors

[1] Corresponding author.

doi:10.1088/1748-0221/11/12/C12016

Contents

1 Setting the stage

A recent development in silicon detector technology is the capability of adding low controlled gain into an otherwise standard silicon sensor [1]. This new type of silicon sensor, the so called Low Gain Avalanche Diodes (LGAD), promises to significantly enhance the capability to measure track arrival times, leading to a dramatic improvement in the capability of silicon arrays. The goal is to simultaneously maintain the high granularity for spatial measurement and the capability for high rate data collection while making very accurate time measurements [2], in fact the time measurement requires very short duration signals allowing even larger data rates than conventional silicon sensors. Not all sensors geometries, thicknesses or gain values are suitable for precise timing measurements: we call Ultra-Fast Silicon Detectors (UFSD) those LGAD sensors optimized for timing measurements [3].

2016 JINST 11 C12016

2 The effect of timing information

The inclusion of timing information in the structure of a recorded event has the capability of changing the way we design experiments, as this added dimension dramatically improves the reconstruction process.

Depending on the type of sensors that will be used, timing information can be available at different stages in the reconstruction of an event. The most complete option is that timing is associated to each point of the track: in this case the electronics needs to be able to accurately measure the time of the hit in each pixel. This option is indeed quite difficult to achieve, due to the massive increase of power consumption that such architecture would require. This increase in power consumption can be avoided by reducing the extension and granularity of the timing information, moving the timing sensors outside the volume of the tracker and instrumenting a dedicated "timing detector". This specific idea has been explored by ATLAS [5] in order to improve Level 1 trigger decision and in the CMS upgrade [6].

Considering a specific situation, at HL-LHC [7] the number of events per bunch crossing will be of the order of 150–200, with an average distance between vertices of 500 micron and a timing rms spread of 150 ps. Considering a vertex separation resolution of 250–300 micron along the beam direction (present resolution for CMS and ATLAS), there will be 10–15% of vertices composed by two events. Without the possibility to separate these vertices using timing information, this overlap will cause a degradation in the precision of the reconstructed variables, and lead to loss of events. We can therefore conclude that timing information at HL-LHC is equivalent of having additional luminosity.

3 Time-tagging detectors

Figure 1 shows the main components of a sensor and its associated electronics able to tag the arrival time of a particle (a time-tagging detector). For a pioneering article on timing see [8] while for an up-to-date review of current trends in electronics see [9]. The sensor, shown as a capacitor with a current source in parallel, is read-out by a pre-amplifier that shapes the signal. The pre-amplifier's output is then compared to a fixed threshold to determine the time of arrival. In the following we will use this simplified model and we will not consider more complex and space-consuming approaches such as waveform sampling. Note that averaging multiple (N) measurements at different threshold values does not lead to an improvement in the time resolution proportional to $1/\sqrt{N}$ since the points are strongly correlated.

There are several effects that contribute to the total value of the time resolution σ_t: (i) electronic noise (Jitter), (ii) Landau amplitude variation (Time Walk) , (iii) Landau non uniform charge deposition (Landau noise), (iv) non uniform drift velocity and weighting field (Signal distortion), and (v) TDC binning:

$$\sigma_t^2 = \sigma_{\text{Jitter}}^2 + \sigma_{\text{Time walk}}^2 + \sigma_{\text{Landau noise}}^2 + \sigma_{\text{Signal distortion}}^2 + \sigma_{\text{TDC}}^2. \tag{3.1}$$

For the sake of clarity, in the following we will assume the contribution of TDC binning to be below 10 ps and therefore it will be ignored. The other terms will be explained in sections 3.1-3.4.

2016 JINST 11 C12016

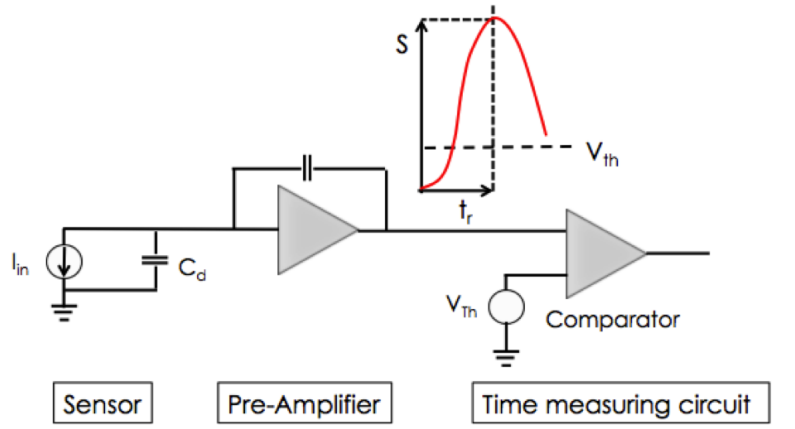

Figure 1. Main components of a detectors able to tag the arrival time of a particle. The time is measured when the signal crosses the comparator threshold V_{th}.

3.1 Jitter

The jitter term represents the time uncertainty caused by the early or late firing of the comparator due to the presence of noise on the signal, it is directly proportional to the noise N of the system and it is inversely proportional to the slope of the signal around the value of the comparator threshold. Assuming a constant slope we can write $dV/dt = S/t_r$ and therefore:

$$\sigma_J = \frac{N}{dV/dt} = \frac{t_r}{S/N}. \tag{3.2}$$

3.2 Time-walk

Time-walk, the unavoidable process by which larger signals cross a given threshold earlier than smaller ones, needs to be corrected by an appropriate electronic circuit. The three most common solutions are: (i) Constant Fraction Discriminator (CFD), which sets the time of arrival of a particle when the signal reaches a given fraction of the total amplitude, (ii) Time over Threshold (ToT), that uses the signal width at a given amplitude to apply an amplitude-dependent correction to compensate for amplitude variations and (iii) Multiple Samplings (MS), where the signal is sampled multiple times, and a fit is used to define the particle time. In the following we will assume that the read-out electronics, using one of these three possibilities, is able to reduce the contribution of time walk to the total time uncertainty to a sub-leading contribution, and therefore it can be ignored. This assumption is motivated by our measurements with time tagging detectors in beam test and laboratory that indicate that the residual contribution is well below the other effects.

3.3 Landau fluctuations: time walk and Landau noise

The ultimate limit to signal uniformity is given by the physics governing energy deposition: the charge distribution created by an ionizing particle crossing a sensor varies on an event-by-event basis. These variations not only produce an overall change in signal magnitude, which is at the root of the time walk effect (section 3.2), but also produce an irregular current signal (Landau noise).

2016 JINST 11 C12016

The left part in figure 2 shows 2 examples of the simulated [10] energy deposition by a minimum ionizing particle, while the right part shows the associated generated current signals and their components. As the picture shows, the variations are rather large and they can severely degrade the achievable time resolution: if we assume to place the discriminator threshold at a given fraction of the total signal, the time at which the signal reaches this value in the two examples differs typically by many tens of picosecond. There are two ways to mitigate this effect: (i) integrating the output current over times longer than the typical spike length and (ii) using thin sensors, as their steeper signal is more immune to signal fluctuations.

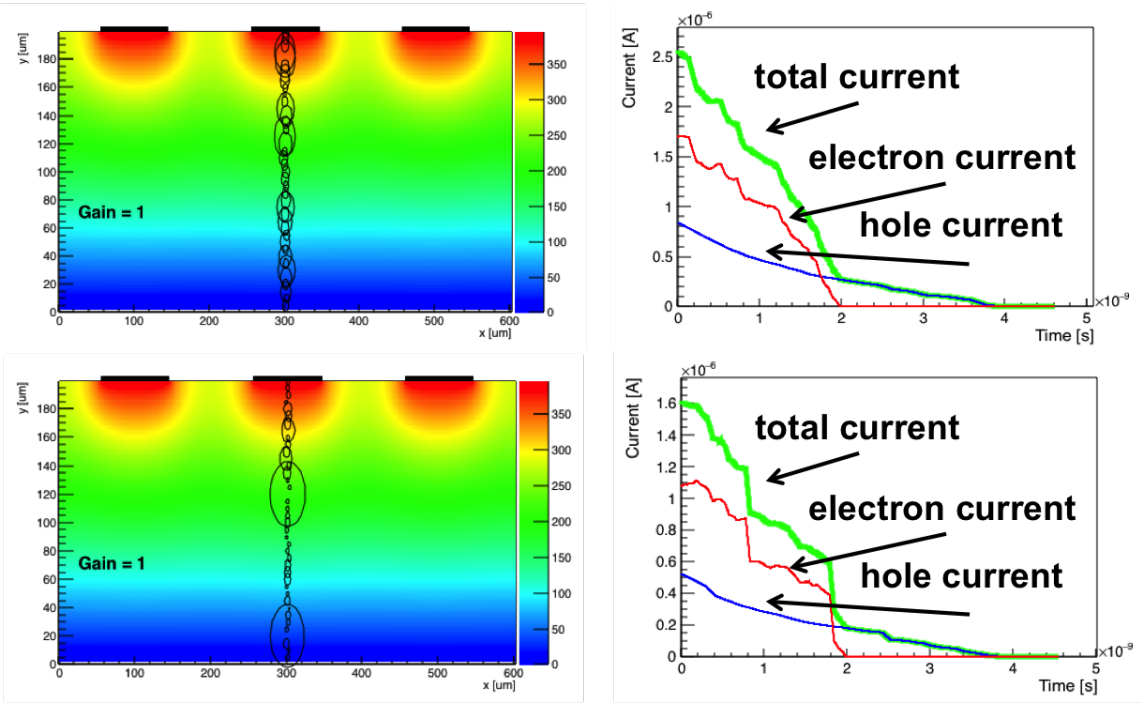

Figure 2. Energy deposits in a silicon detectors and the corresponding current signals. The differences in charge depositions generate current signals that differs significantly on an event-by-event basis. These differences results in a contribution to the overall time resolution that can be the dominant factor.

3.4 Signal Distortion: non uniform weighting field and not saturated drift velocity

In every particle detector, the shape of the induced current signal can be calculated using the Shockley-Ramo [11, 12] theorem that states that the current induced by a charge carrier is proportional to its electric charge q, the drift velocity v and the weighting field E_w, equation (3.3):

$$i = -q\vec{v} \cdot \vec{E_w}. \tag{3.3}$$

This equation indicates several key points in the design of sensors for accurate timing, shown in figure 3:

- the drift velocity needs to be constant throughout the volume of the sensor. Non-uniform drift velocity induce variations in signal shape as a function of the hit position, figure 3 a), spoiling

2016 JINST 11 C12016

the overall time resolution. The easiest way to obtain uniform drift velocity throughout the sensor is to have an electric field high enough to move the carriers with saturated drift velocity.

- the weighting field E_w represents the capacitive coupling of a charge e to the read-out electrode. If this coupling depends on the impinging particle position along the strip pitch, figure 3 b), the signal shape would be different depending on the hit position, spoiling the time resolution. Strips need to have their width very similar to the pitch, and be larger than the signal thickness: width ~ pitch, both much larger than thickness.

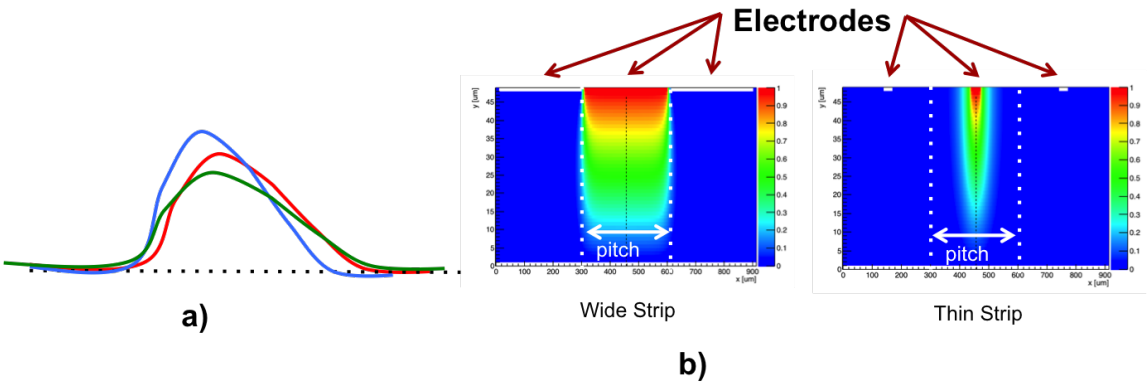

Figure 3. a) The signal shape depends on the velocity of the electron-hole pairs generated by the impinging particle: in case of non saturated drift velocity, the output signal will depend on the impinging position. b) Weighting field for two configurations: (left) Wide strips, (right) Thin strips. In "thin strips", the weighting field is such that particles hitting near the center of the strip generate a much steeper and earlier signal.

3.5 The t_0 problem

In systems where the weighting field is not constant over the sensor volume, figure 3 b) right side, there is an additional source of time uncertainties: the charge carriers created by the impinging particle have to drift from the impact point to the region of high weighting field before generating a significant signal. In silicon, electrons with saturated velocity move about 1 μm in 10 picosecond and therefore particles hitting on the side of the thin strip have signals that start many tens of picosecond later. This effect can easily become the dominant source of time uncertainty.

3.6 Roadmap

The integration of time-tagging capabilities into a position sensor produces a steep increase in system complexity. Part of this complexity can be addressed by smart architectures, new technological nodes (for example 65 nm) allowing higher circuit densities and new chip designs, however the present bottlenecks inherent to hybrid systems, having sensors and electronics built on separated substrates, will ultimately limit the complexity and drive the cost. Most likely the real turning point of 4D tracking will happen when monolithic technology will be mature enough to allow integrating the sensor and the electronics in the same substrate, reducing interconnections and keeping the capacitance of each sensor low. As we are deciding now (2016) the choices for HL-LHC (2025),

2016 JINST 11 C12016

this evolution will not be used at HL-LHC, but it will probably appear first in smaller experiments, and then be used on larger scales.

4 Design of a 4D tracker using Ultra-Fast Silicon Detectors

4.1 LGAD - Low-Gain Avalanche Diodes

Standard silicon detectors can be used in timing applications, provided the sensor geometry is appropriate. Currently the NA62 experiment [13] is employing a track-timing detector, the so called Gigatracker, that uses 200-micron thick sensors with 300×300 micron pixels. The expected time resolution is around $\sigma_t \sim 150$ ps. Recently [14], employing an extremely low noise new circuit, a resolution of $\sigma_t \sim 105$ ps has been reached using a 100-micron thick, 4 mm^2 square pad sensor. Standard silicon sensors have therefore the capability of reaching good time resolutions, however it is rather difficult to reach resolutions better than $\sigma_t \sim 80$–100 ps given their small signal. The natural evolution of this problem is therefore to manufacture silicon sensors with a larger output signal: the Low-Gain Avalanche Diodes (LGAD).

LGAD is a new concept in silicon detector design, merging the best characteristics of standard silicon sensors with the main feature of APDs [15–19], however without the additional problems affecting high gain devices (SiPM and APDs). A SiPM sensor is a collection of many small pixels working in Geiger mode, and it needs several pixel cells to fire at the same time in order to have a large signal: since an impinging particle fires a single pixel, the SiPM signal from a MIP is too small to be used efficiently. APDs, given their high gain, produce a very large signal in response to a MIP particle, ideal for timing, however they are difficult to segment, and their high gain, as explained in section 4.4, makes them very noisy as soon as the leakage current increases.

Charge multiplication in silicon sensors happens when the charge carriers are in electric fields of the order of $E \sim 300$ kV/cm. Under this condition the electrons (and to less extent the holes) acquire sufficient kinetic energy that are able to generate additional e/h pairs. A field value of 300 kV/cm can be obtained by implanting an appropriate charge density that locally generates very high fields ($N_D \sim 10^{16}$/cm^3). The gain has an exponential dependence on the electric field $N(l) = N_o e^{\alpha(E)l}$, where $\alpha(E)$ is a strong function of the electric field and l is the path length inside the high field region. The additional doping layer present at the n-p junction in the LGAD design, figure 4, generates the high field necessary to achieve charge multiplication.

According to our simulation program Weightfield2[1] (WF2), LGAD have the potentiality of replacing standard silicon sensors in almost every application, with the added advantage of having a large signal dV/dt and therefore being able to measure time accurately. In the following, we will use the name of "Ultra-Fast Silicon Detectors" (UFSD) to indicate LGAD sensors optimized for timing performances.

4.2 The effect of charge multiplication

Using WF2, we can simulate the output signal of UFSD sensors as a function of many parameters, such as the gain value, sensor thickness, electrode segmentation, and external electric field. Figure 5 shows the simulated current, and its components, for a 50-micron thick detector. The initial electrons

[1]Open source code, link at cern.ch/nicolo.

2016 JINST 11 C12016

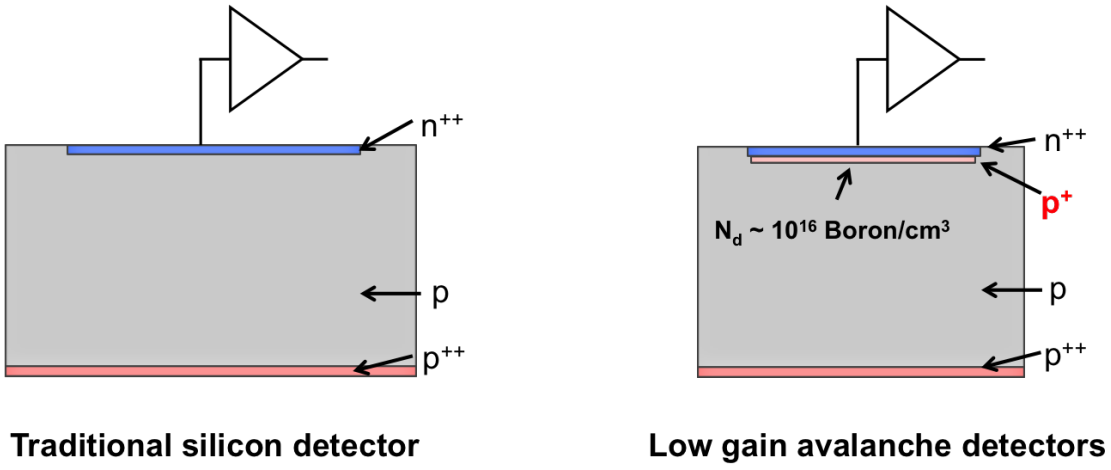

Figure 4. Schematic of a traditional silicon diode (left) and of a Low-Gain Avalanche Diode (right). The additional p^+ layer underneath the n^{++} electrode creates, when depleted, a large electric field that generates charge multiplications.

(red), drifting toward the n^{++} electrode, go through the gain layer and generate additional e/h pairs. The gain electrons (violet) are readily absorbed by the cathode while the gain holes (light blue) drift toward the anode and they generate a large current.

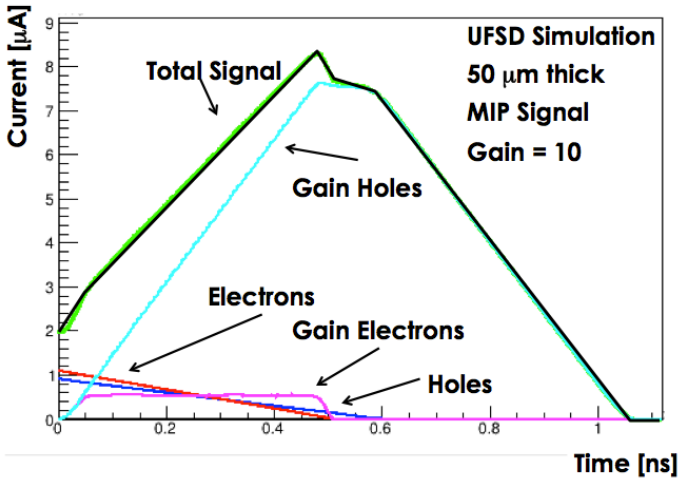

Figure 5. UFSD simulated current signal for a 50-micron thick detector. The evolution of the signal is governed by the initial electrons ("Electrons") reaching the multiplication layer and generating the "Gain Electrons" and "Gain Holes". The gain electrons are immediately absorbed by the n^{++} electrode, and therefore their contribution to the current in negligible. The gain holes, on the contrary, drifting towards the p^{++} contact, generate a large current with a large slew rate.

The gain dramatically increases the signal amplitude, producing a much higher slew rate. The value of the current generated by a gain G can be estimated in the following way: (i) in a given time interval dt, the number of electrons entering the gain region is $75vdt$ (assuming 75 e/h pairs per micron); and (ii) these electrons generate $dN_{\text{Gain}} = 75vdtG$ new e/h pairs. Using again Ramo's

2016 JINST 11 C12016

theorem, the current induced by these new charges is given by:

$$di_{\mathrm{Gain}} = dN_{\mathrm{Gain}} q v_{\mathrm{sat}} \frac{1}{d} = 75 q v_{\mathrm{sat}} \frac{G}{d} dt, \tag{4.1}$$

which leads to the following expression for the current slew rate:

$$\frac{di_{\mathrm{Gain}}}{dt} = 75 q v_{\mathrm{sat}} \frac{G}{d}. \tag{4.2}$$

Equation (4.2) demonstrates a very important feature of UFSD: the current slew rate increase due to the gain mechanism is proportional to the ratio of the gain value over the sensor thickness (G/d), therefore thin detectors with high gain provide the best time resolution. Specifically, assuming a geometry with electrodes much larger than their separation, the maximum signal amplitude is controlled only by the gain value, while the signal rise time only by the sensor thickness, figure 6, left side.

Using WF2 we have cross-checked this prediction simulating the slew rate for different sensors thicknesses and gains, figure 6 right side: the slew rate in thick sensors, 200- and 300-micron, is a factor of ~ 2 higher than that of traditional sensors, while in thin detectors, 50- and 100-micron thick, the slew rate is 5-6 times larger.

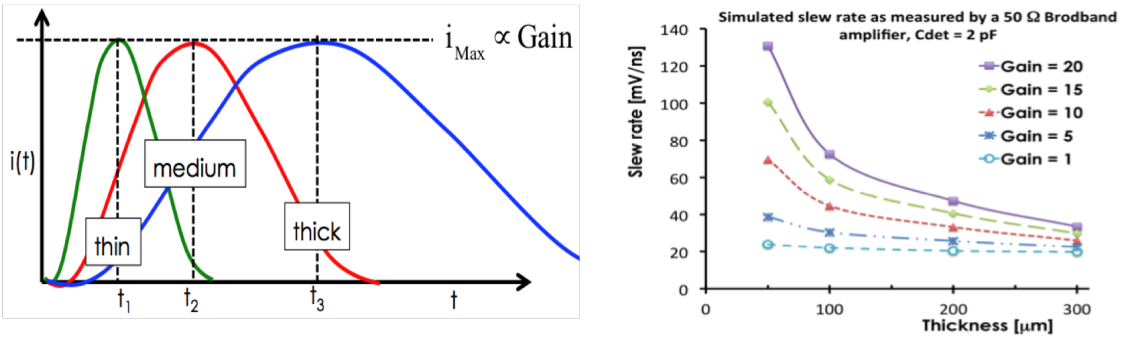

Figure 6. Left side: in UFSD the maximum signal amplitude depends only on the gain value, while the signal rise time only on the sensor thickness: sensors of 3 different thicknesses (thin, medium, thick) with the same gain have signals with the same amplitude but with different rise time. Right side: simulated UFSD slew rate as a function of gain and sensor thickness. Thin sensors with even moderate gain (10–20) achieve a much larger slew rate than traditional sensors (gain = 1).

4.3 Landau noise in UFSD sensors

With WF2 we have studied in detail the effect of Landau noise on time resolution, figure 7. The picture shows several important effects: (i) Landau noise sets a physical limit to the precision of a given sensor: this limit is of the order of 20 ps in thin sensors, and much larger for thicker sensors, (ii) Landau noise is minimized by setting the comparator threshold as low as possible, (iii) thin detectors are less prone to Landau noise.

4.4 Shot Noise in UFSD sensors

Shot noise arises when charge carriers cross a potential barrier, as it happens in silicon sensors. In sensors such as UFSD or APD this effect is enhanced by the gain and for this reason shot noise

2016 JINST 11 C12016

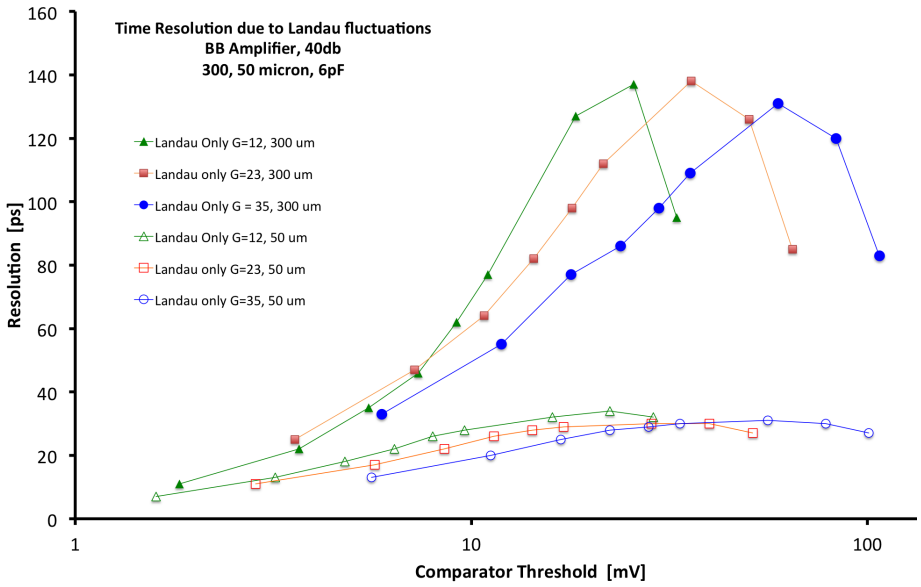

Figure 7. Effect of Landau noise on time resolution. The plot shows three effects: (i) Best results are obtained for thin sensors, (ii) given a thickness and a gain, the Landau noise is minimized by placing the CFD threshold as low as possible, and (iii) the value of the gain does not have a strong impact on the Landau noise.

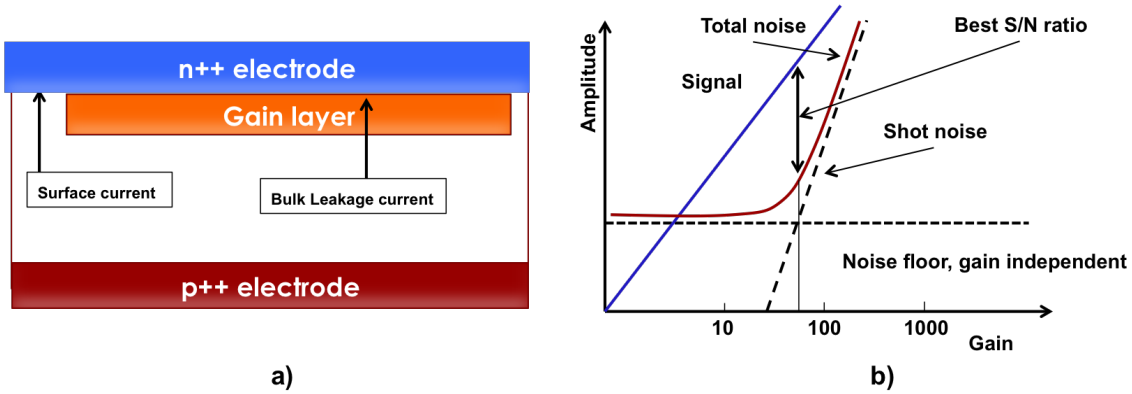

Figure 8. a) Sketch of the shot noise mechanism in sensors with internal gain: bulk current is multiplied by the gain, while surface current is not. b) Dependance of the current and noise amplitude as a function of gain: the signal increases linearly with gain while the noise at first is constant, and then increases faster than the signal when Shot noise becomes the dominant contribution. [20].

can be the dominant source of noise for this type of detectors. As shown in figure 8 a), the sensor leakage current is the sum of two components: (i) surface current, that does not go through the multiplication layer, and (ii) bulk current, that is multiplied by the gain mechanism.

When carriers undergo multiplication, there is an additional mechanism that enhances shot noise: multiplication is a statistical process, therefore some carriers multiply more than others, causing an increase in noise, the so called *excess noise factor*, ENF. This effect is in addition to the increase in noise due to the gain value that simply multiply the leakage current. ENF causes a

2016 JINST 11 C12016

very peculiar effect: in device with gain, as the gain increases the ratio signal/noise (S/N) becomes smaller since shot noise increases faster than the signal, figure 8 b). In order to obtain a beneficial effect from the gain mechanism it is therefore necessary to have a gain value small enough (gain ≤ 20) that the signal increases while the noise increment is small enough to be in the shadow of the electronic noise floor. Shot noise is normally smaller than the electronic noise floor for un-irradiated sensors, but it can become the dominant source of noise for irradiated detectors. Figure 9 shows the value of shot noise for a 4 mm^2 50-micron thick silicon sensor, assuming a 2-ns long integration time. In the plots the electronic noise is assumed to be 450 e^- (ENC). Figure 9 a) demonstrates the dramatic effect of gain on shot noise, whereas in figure 9 b) is shown the effect of temperature (leakage current decreases a factor of 2 every 7 degrees).

Figure 9 demonstrates that shot noise can become the most important source of noise for irradiated sensors with gain, and suggests that low gain and low temperature can keep this effect under control. Additionally, shot noise can be kept under control by keeping the volume under each each pixel/strip small, as leakage current depends on the volume per electrode: $I_{\text{Leak}} = \alpha * \Phi * V$, with $\alpha = 3 \cdot 10^{-17} cm^{-1}$ and Φ the particle fluence in n_{eq}/cm^2.

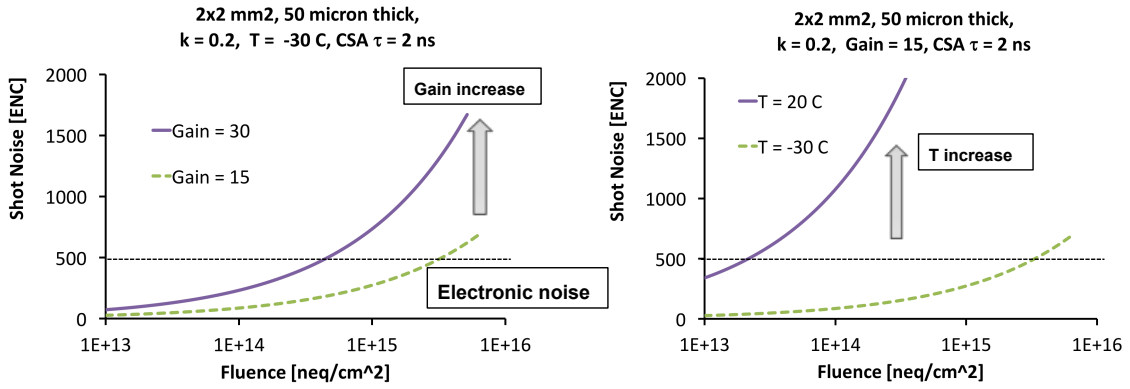

Figure 9. a) Shot noise increase as a function of fluence for two different gain values. b) Shot noise increase as a function of fluence for two different temperature values

4.5 Interplay of UFSD current rise time, detector capacitance and read-out input impedance

The charges collected on the read-out electrode of the sensor move to the input of the read-out electronics with a time constant given by the product of the detector capacitance C_{det} and the read-out input impedance R_{in} : $t_{\text{RC}} = R_{\text{in}} C_{\text{det}}$. In order not to slow down the UFSD current rise time t_{Cur}, the time constant t_{RC} has to be shorter or, at most, of the same order of t_{Cur}: this constraint is strongly linking sensor and electronics designs. The third component determining the signal rise time at the output of the pre-amplifier t_{Rise} is the amplifier's own rise time t_{Amp}. We can therefore identify 3 distinct effects that influence the signal slew rate at the comparator input, eq. (4.3): (i) the signal rise time t_{Cur} that depends on the properties of the sensor, (ii) the $t_{\text{RC}} = R_{\text{in}} C_{\text{det}}$ time constant, and (iii) the amplifier rise time t_{Amp}, which should be matched to t_{Cur} and t_{RC} to minimize the noise of the amplifier:

$$t_{\text{Rise}} = \sqrt{t_{\text{Cur}}^2 + t_{\text{RC}}^2 + t_{\text{Amp}}^2}. \tag{4.3}$$

2016 JINST 11 C12016

4.6 Radiation effect in UFSD sensors

Radiation damage causes three main effects: (i) decrease of charge collection efficiency, (ii) increase of leakage current, and (iii) changes in doping concentration.

Decrease of charge collection efficiency. Charge collection efficiency (CCE) measures the fraction of charge carriers that are not trapped by lattice defects. This fraction decreases with increasing radiation levels (with differences depending on the type of silicon and type of irradiation) and with increasing drift length. As a rule of thumb, for irradiation levels around 10^{15} n_{eq}/cm^2, the mean free path in silicon is around 50 micron. Figure 10 shows the simulated [21] signal changes as a function of radiation level for a 50-micron thick sensor: the effect is rather small up to a fluence of 10^{15} n_{eq}/cm^2, and it becomes important above a fluence of $5 \cdot 10^{15}$ n_{eq}/cm^2. Interestingly, the initial edge of the signal, used for timing, it is not affected much.

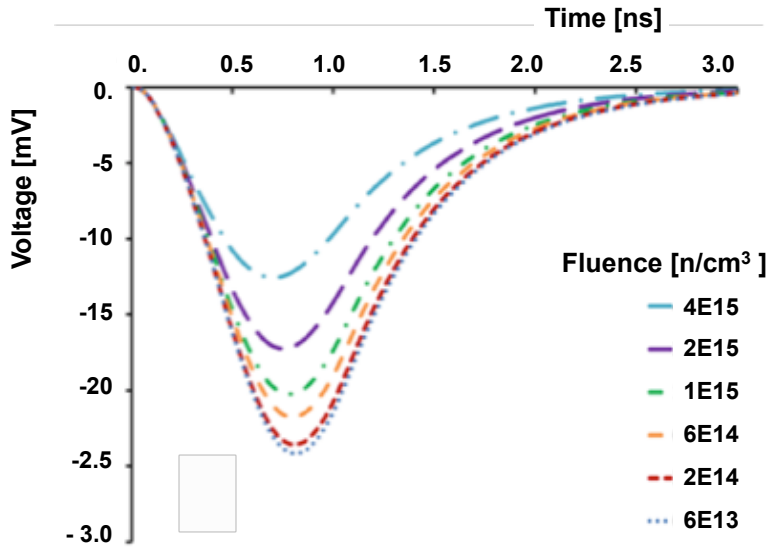

Figure 10. Signal change in a 50-micron silicon sensor as a function of irradiation levels (the only effect considered in this plot is charge trapping).

Increase of leakage current. An increase in leakage current causes two important effects: (i) a larger noise, as explained in section 4.4, and (ii) a change in the apparent doping concentration. This second effect can be quite important, and it is presently under intense study.

Changes in doping concentration. UFSD sensors have shown a decrease of gain values for fluences above 10^{14} n_{eq}/cm^2, with a complete disappearance of the gain at 10^{15} n_{eq}/cm^2. This effect has not been understood yet, but there are two possible explanations: (i) an inactivation of acceptors due to radiation defects [22], and (ii) a dynamic reduction of the gain layer doping due to charge trapping. There are currently three research paths in the investigation of gain reduction, aiming at establishing a radiation hard design for UFSD: (i) change the dopant of the p-type gain layer from Boron to Gallium, as Gallium, given its higher mass, has been shown to be less prone to become electrically inactive due to interstitial capture [23], (ii) development of very thin sensors,

Table 1. Timing resolution for single ($N = 1$), doublet ($N = 2$) and triplets ($N = 3$) of UFSD at bias voltages of 200 V and 230 V.

V bias [V]	200 V	230 V
$\sigma_t(N = 1)$	34.1 ps	27.4 ps
$\sigma_t(N = 2)$	24.2 ps	19.8 ps
$\sigma_t(N = 3)$	19.9 ps	16.4 ps

to decrease the amount of leakage current and therefore trapping, and (iii) doping of the gan layer using Carbon [23].

5 Productions and Performances of Ultra-Fast Silicon Sensors

The first publication containing measurements of LGAD sensors has been presented in 2014 by the Centro Nacional de Microelectrónica (CNM) Barcelona [16] while the first production of thin UFSD (50 μm) by CNM was presented in 2016 [24]. First beam test results on thin UFSD manufactured by CNM have been obtained in 2016 [25]. The Fondazione Bruno Kessler (FBK) has also designed [17], and produced LGAD sensors, up to now only 300-micron thick [26]; first FBK production of thin LGAD is expected in early 2017. At the 2016 IEEE conference it was announced that Hamamatsu photonics has produced successfully thin UFSD (50- and 80-micron thick). In the past 3 years CNM has manufactured a variety of LGAD designs, exploring different substrates (float zone (FZ), silicon-on-insulator (SoI), epitaxial (epi) with high and medium resistivity), reaching a well-controlled manufacturing capability. FBK has manufactured a single run of very high quality, exploring traditional LGAD design, segmented p-side read-out and AC coupling read-out.

5.1 Results from 50-micron thick UFSD

In this section we report on the results obtained in a beam test at CERN with π-mesons with a momentum of 180 GeV/c. Several $1.2 \times 1.2\,\mathrm{mm}^2$ UFSD read-out by a fully custom broadband amplifier and a trigger board comprising of a SiPM coupled to a quartz bar were used [25]. This beam test, coupled with complementary laser measurements performed in our laboratories, provides the opportunity to perform detailed studies of the mechanisms governing UFSD time resolution and to compare these measurements to our simulation.

The left side of figure 11 shows typical beam test signals, and the right side shows a comparison between data and WF2, demonstrating the capability of WF2 to reproduce the UFSD beam test signals accurately. The signals are very fast, with low noise and large slew rate, ideal for timing studies. The time resolution of each sensor and that of the SiPM has then been obtained from the time differences between pairs of UFSD and between each UFSD and the SiPM, yielding two values for each UFSD. The time resolution of combined UFSD has been evaluated as the difference between the average time of two or three UFSD and the SiPM, table 1. The results of table 1 agree well with the expected $\sigma(N) = 1/\sqrt{N}$ behaviour, demonstrating that the 3 sensors are of equal high quality. The timing resolution of a single UFSD is measured to be 34 ps for 200 V bias and 27 ps for 230 V bias. A system of three UFSD has a measured timing resolution of 20 ps for a bias of 200 V, and 16 ps for a bias of 230 V.

2016 JINST 11 C12016

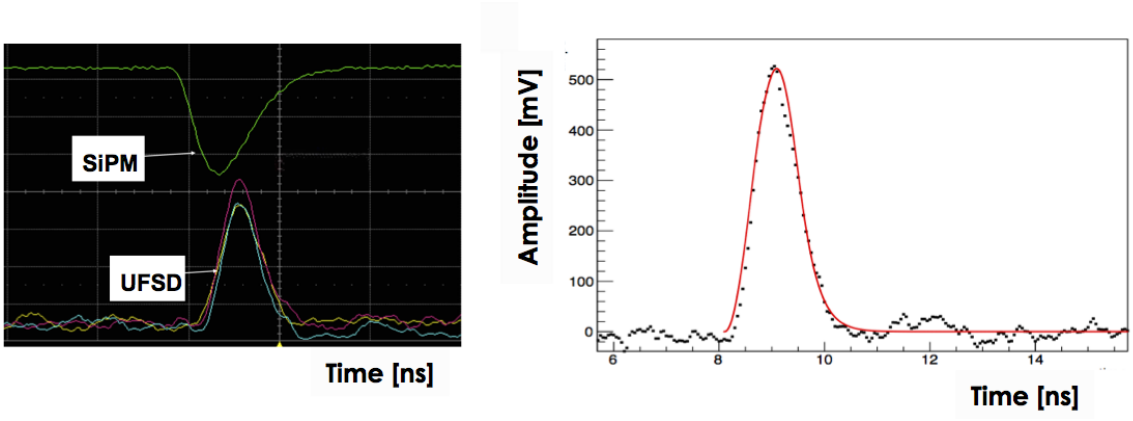

Figure 11. Left side: signals of a beam test event showing the coincidence of 3 50-micron thick UFSD sensors and the SiPM trigger counter. Right side: data — WF2 simulation (solid line).

6 Summary

In the past 3 years we have designed, produced and tested a new type of silicon detector, characterized by a controlled, low internal gain (Low Gain Avalanche Detector). Given the low gain values, these sensors are a cross-bred between traditional silicon sensors and APDs, enjoying the best characteristics of both families. The LGAD principle allowed us designing segmented silicon sensors with added timing capabilities, the so called Ultra-Fast Silicon Detectors, able of a time resolution of $\sigma_t \sim 35$ ps. In the next years we will pursue the further development of the UFSD design, aiming at a full tracker system able to provide complete 4D information.

Combining the information presented in the paper, it is clear that not all geometries can be used in time tagging detectors. The most important points to have a detector with excellent time resolution are:

- High field to have saturated velocity.
- Large electrodes to avoid the t_o problem.
- Geometries as similar as possible to parallel plate capacitors, offering uniform electric and weighting fields
- High velocity carriers, to have large dV/dt
- Low capacitance, to minimize jitter
- Small volumes, to minimize leakage current and therefore Shot noise

Acknowledgments

We thank our collaborators within RD50, ATLAS and CMS who participated in the development of UFSD. Our special thanks to the technical staff at UC Santa Cruz, INFN Torino, CNM Barcelona and FBK Trento. This work was partially performed within the CERN RD50 collaboration.

2016 JINST 11 C12016

The work was supported by the United States Department of Energy, grant DE-FG02-04ER41286. Part of this work has been financed by the European Union's Horizon 2020 Research and Innovation funding program, under Grant Agreement no. 654168 (AIDA-2020) and Grant Agreement no. 669529 (ERC UFSD669529), and by the Italian Ministero degli Affari Esteri and INFN Gruppo V.

References

[1] G. Pellegrini et al., *Technology developments and first measurements of Low Gain Avalanche Detectors (LGAD) for high energy physics applications*, *Nucl. Instrum. Meth.* **A 765** (2014) 24.

[2] H.F.-W. Sadrozinski, *Exploring charge multiplication for fast timing with silicon sensors*, talk given at *20th RD50 Workshop*, Bari, Italy, May 30 – June 1 2012.

[3] N. Cartiglia et al., *Design Optimization of Ultra-Fast Silicon Detector*, *Nucl. Instrum. Meth.* **A 96** (2015) 141.

[4] N. Neri et al., *4D fast tracking for experiments at HL-LHC*, in proceedings of *Pixel 2016 International Workshop*, Sestri Levante, Genova, Italy, September 5–9 2016.

[5] ATLAS upgrade project, https://cds.cern.ch/record/2055248/files/LHCC-G-166.pdf.

[6] CMS upgrade project, https://cds.cern.ch/record/2020886?ln=en&asof=2099-12-31.

[7] HL-LHC, http://dx.doi.org/10.5170/CERN-2015-005.

[8] H. Spieler, *Fast timing methods for semiconductor detectors*, *IEEE Trans. Nucl. Sci.* 29 (1982) 1142.

[9] A. Rivetti, *Fast front-end electronics for semiconductor tracking detectors: Trends and perspectives*, in proceedings of *HSTD9*, Hiroshima, Japan, *Nucl. Instrum. Meth.* **A 765** (2014) 202.

[10] F. Cenna et al., *Weightfield2: A fast simulator for silicon and diamond solid state detector*, *Nucl. Instrum. Meth.* **A 796** (2015) 149.

[11] W. Shockley, *Currents to Conductors Induced by a Moving Point Charge*, *J. Appl. Phys.* **9** (1938) 635.

[12] S. Ramo, *Currents Induced by Electron Motion*, *Proc. IRE* **27** (1939) 584.

[13] E. Martin et al., *Review of results for the NA62 gigatracker read-out prototype*, 2012 *JINST* **7** C03030.

[14] M. Benoit, R. Cardarelli, S. Débieux, Y. Favre, G. Iacobucci, M. Nessi et al., *100 ps time resolution with thin silicon pixel detectors and a SiGe HBT amplifier*, arXiv:1511.04231.

[15] P. Fernandez et al., *Simulation of new p-type strip detectors with trench to enhance the charge multiplication effect in the n-type electrodes*, *Nucl. Instrum. Meth.* **A 658** (2011) 98.

[16] G. Pellegrini et al., *Technology developments and first measurements of Low Gain Avalanche Detectors (LGAD) for High Energy Physics applications*, *Nucl. Instrum. Meth.* **A 765** (2014) 12.

[17] G.-F. Dalla Betta et al., *Design and TCAD simulation of double-sided pixelated low gain avalanche detectors*, *Nucl. Instrum. Meth.* **A 796** (2015) 154.

[18] H.-W. Sadrozinski et al., *Sensors for ultra-fast silicon detectors*, *Nucl. Instrum. Meth.* **A 765** (2014) 7.

[19] H.F.W. Sadrozinski et al., *Ultra-fast silicon detectors*, *Nucl. Instrum. Meth.* **A 730** (2013) 226.

[20] Hamamatsu Photonics, *Characteristics and use of SiAPD*, Technical Information SD-28.

[21] B. Baldassarri et al., *Signal formation in irradiated silicon detectors*, *Nucl. Instrum. Meth.* **A**, in press.

2016 JINST 11 C12016

[22] G. Kramberger et al., *Radiation effects in Low Gain Avalanche Detectors after hadron irradiations*, 2015 *JINST* **10** P07006.

[23] RD50 collaboration, http://rd50.web.cern.ch/rd50/.

[24] M. Carulla et al., *First LGAD fabrication of 50 μm SOI wafers at CNM for the HGTD*, talk given at *28th RD50 Workshop*, Torino, June 7th 2016.

[25] N. Cartiglia et al., *Beam test results of a 15 ps timing system based on ultra-fast silicon detectors*, submitted to *Nucl. Instrum. Meth.* **A** [arXiv:1608.08681].

[26] A. Staiano, *New Developments in the Design and Production of Low-Gain Avalanche Detectors*, in *IEEE Nuclear Science Symposium and Medical Imaging Conference*, Strasburg, 2016, contribution in print.

2016 JINST 11 C12016